# The enhancing effect of $Co^{2+}$ on propane non-oxidative dehydrogenation over supported $Co/ZrO_2$ catalysts

Qiyang Zhang[a†], Yuming Li[a,b†], Tatiana Otroshchenko[a], Vita A. Kondratenko[a], Kai Wu[a,b], Elizaveta A. Fedorova[a], Dmitry E. Doronkin[c], Stephan Bartling[a], Henrik Lund[a], Guiyuan Jiang[b,*], Evgenii V. Kondratenko[a,*]

[a]*Leibniz-Institut für Katalyse e.V., Albert-Einstein-Str. 29a, D-18059 Rostock, Germany*

[b]*State Key Laboratory of Heavy Oil Processing, China University of Petroleum, Beijing, 102249*

[c]*Institute for Chemical Technology and Polymer Chemistry, and Institute of Catalysis Research and Technology, Karlsruhe Institute of Technology, Kaiserstr. 12, D-76131, Karlsruhe, Germany*

*To whom correspondence should be addressed. E-mail addresses: jianggy@cup.edu.cn (GJ), Evgenii.kondratenko@catalysis.de (EVK)

† These authors contributed equally

**Abstract**

Due to the increased production of shale gas containing propane, the share of non-oxidative propane dehydrogenation (PDH) in the large-scale production of propene is expected to continue to grow. There are, however, some ecofriendly and cost shortcomings associated with the currently applied Cr- or Pt-containing catalysts. Against this background, we present here $Co/ZrO_2$ alternatives and reveal the fundamentals affecting their activity, which can be used for purposeful catalyst design. $Co^{2+}$ species homogeneously distributed within the lattice of $ZrO_2$ significantly increase the activity of coordinatively unsaturated $Zr^{4+}$ for the PDH reaction. The increase is caused by accelerating both the cleavage of CH bonds in propane and the recombination of surface H species, with the latter reaction being the rate-limiting step. The best-performing catalyst outperformed an analogue of commercial K-$CrO_x/Al_2O_3$ in terms of the rate of propene formation and demonstrated durable performance over a series of 10 PDH/regeneration cycles under industrially relevant conditions. It also outperformed most previously developed Co-containing catalysts in terms of propene productivity. The space-time yield of propeneformation achieved at 57% equilibrium propane conversion at 550°C was 0.71 $kg \cdot h^{-1} \cdot kg_{cat}^{-1}$.

**Keywords:** propane, propene, dehydrogenation, cobalt, zirconia, synergistic effect

## 1 Introduction

Propene is one of the most important basic petrochemicals widely used for the manufacture of polypropylene, solvents, acrylic acid, etc[1-4]. Current large-scale propene production routes include steam or fluid catalytic cracking of various oil fractions[5], metathesis of ethene with 2-butenes[6-10] and non-oxidative propane dehydrogenation (PDH)[11]. The latter on-purpose approach has become more attractive due to the exploitation of shale gas[12]. Catalysts with supported $CrO_x$ or Pt species are used in large-scale PDH processes[2, 4]. However, the high cost of Pt and the environmental impact of Cr(VI) compounds have prompted both academia and industry to develop alternative PDH catalysts free of such limitations.

Recently, Co-based catalysts with highly dispersed $CoO_x$ and/or metallic Co species have attracted more attention due to the low cost of this metal and high efficiency for CH bond activation in light alkanes[13-23]. Bulk $ZrO_2$-based catalysts are also active and selective for the PDH reaction[24, 25]. Coordinatively unsaturated Zr cations ($Zr_{cus}$) were concluded to be involved in the cleavage of CH bonds in $C_3H_8$. Their concentration depends on the reducibility of $ZrO_2$. This material property can be controlled through (i) promoting of $ZrO_2$ with an oxide of a metal with oxidation state lower than 4+, (ii) the deposition of tiny amounts of metallic Cu, Rh, or Ru species, and (iii) the kind of $ZrO_2$ phase and its crystallite size. A synergistic effect between $Zr_{cus}$ and $CrO_x$ in bulk and supported $CrZrO_x$-based catalysts has been demonstrated in terms of their PDH activity[26, 27]. Although such catalysts outperform an analogue of commercial K-$CrO_x/Al_2O_3$ in this respect, they are still environmentally harmful.

Motivated by the outstanding PDH performance of $ZrO_2$-based and Co-containing catalysts, we decided to explore the potential of Co-promoted $ZrO_2$ materials. Our specific objectives were (i) to elucidate the kind of catalytically active sites, and (ii) to identify the rate-limiting step and the option(s) for accelerating this pathway. To be successful in this regard, we applied complementary characterization techniques including XRD, TEM, $H_2$-TPR, UV-vis spectroscopy, XPS and X-ray absorption spectroscopy to characterize the phase composition, redox properties of the prepared catalysts. Through temporal analysis of products and temperature-programmed surface reaction, we revealed that $H_2$ formation through recombination of two hydrogen atomic species is the rate-limiting step in the PDH reaction. The rate of this step is affected by the presence of $Co^{2+}$ in the lattice of $ZrO_2$. This knowledge provides a basis for the rational design of $ZrO_2$-based catalysts and can be extended to other non-reducible metal oxides capable of releasing their lattice oxygen at high temperatures. From an application viewpoint, the developed catalysts show comparable activity with an analogue of a commercial K-$CrO_x/Al_2O_3$ catalyst and are durable under industrially relevant reaction conditions.

## 2 Experimental part

### *2.1 Catalyst Synthesis*

To synthesize $Co/ZrO_2$ catalysts with different Co loadings, monoclinic $ZrO_2$ (99%, Daiichi Kigenso Kagaku Kogyo Co) was impregnated (incipient wetness impregnation) with an aqueous solution of $Co(NO_3)_2 \cdot 6H_2O$ followed by drying at 100°C for 12 h and calcination in flowing air at 550°C for 6 h. The loading of cobalt in the catalysts was in the range between 0.1 and 3 wt%. The samples obtained have been designated as $xCo/ZrO_2$, where "x" stands for the percentage by weight of cobalt. Differently loaded $Co/SiO_2$ materials were prepared using

$SiO_2$ (Davisil, grade 646, Sigma-Aldrich) as support according to the above-mentioned procedure and named as $xCo/SiO_2$.

An analogue of commercial $K\text{-}CrO_x/Al_2O_3$ catalyst was prepared according to the protocol described in the literature[27]. Briefly, two aqueous solutions with the required amounts of $CrO_3$ and KOH were separately prepared and then mixed. Hereafter, $Al_2O_3$ (Saint-Gobain NorPro) was impregnated with the resulting solution. The catalyst precursor was dried at 120 °C over night and calcined at 760°C for 4 h. The nominal concentration of $Cr_2O_3$ and $K_2O$ in the resulting catalyst are 19.7 wt.% and 0.93 wt.% respectively.

### *2.2 Catalyst Characterization*

UV-vis spectroscopic measurements of all catalysts were carried out using an Avantes spectrometer (AvaSpes-2048-USB2-RM) equipped with a high-temperature reflection UV-vis probe, an Ava-Light-DH-S-BAL deuterium-halogen light source and a CCD array detector. The probe consisting of six radiating optical fibers and one reading fiber was threaded through the furnace to face the wall of the quartz tubular reactor at the position where the catalyst (200 mg) was positioned. The UV-vis spectra were recorded at room temperature in the range from 200-1100 nm. Barium sulfate (99.998%, Aldrich) was used as a white standard.

Temperature-programmed reduction tests with $H_2$ ($H_2$-TPR) were carried out in an in-house developed setup containing eight individually heated continuous-flow fixed-bed quartz reactors. This set-up was also used for temperature-programmed desorption tests with ammonia ($NH_3$-TPD) and temperature-programmed surface reaction ($C_3H_8$-TPSR) measurements with $C_3H_8$.

For $H_2$-TPR tests, 100 mg of each sample were heated in flowing air to 500°C for 1 h, cooled down to room temperature and purged with Ar for 15 min. Hereafter, the catalysts were heated in a flow of 5vol% $H_2$ in Ar (10 mL·min$^{-1}$) up to 900°C with a heating rate of 10 K·min$^{-1}$. An on-line mass spectrometer (Pfeiffer Vacuum OmniStar GSD 320) was used to record signals at *m/z* of 2 ($H_2$) and 40 (Ar), with the latter signal being a reference standard.

Before $NH_3$-TPD tests, each sample (50 mg) was calcined in flowing air at 550°C for 1 h, flushed with Ar (10 mL·min$^{-1}$) for 15min, reduced with 40vol%$H_2$/Ar (10 mL·min$^{-1}$) for 30 min, cooled down to 120°C, and finally purged with Ar for 15 min. Hereafter, the treated materials were exposed to a flow of 1vol% $NH_3$ in Ar (10 mL·min$^{-1}$) at 120°C for 1 h, flushed with Ar for 5 h to remove weakly bound $NH_3$, and cooled down to 80°C in the same flow. Then, they were heated in Ar flow up to 900°C with a heating rate of 10 K·min$^{-1}$. Desorbed ammonia was registered using an on-line mass spectrometer (Pfeiffer Vacuum OmniStar GSD 320). The signals at *m/z* of 15 (NH) and 40 (Ar) were recorded.

Before starting $C_3H_8$-TPSR tests, all catalysts (50 mg for each sample) were calcined at 500 °C in flowing air for 1 h and then cooled down to 300 °C. Hereafter, the catalysts were flushed with Ar for 30 min and exposed to a flow of $C_3H_8$/Ar=10/90 (10 mL·min$^{-1}$). The temperature was initially kept at 300°C for 15 min to stabilize mass spectroscopic signals. Then, the catalysts were heated up to 600°C with a heating rate of 10 K·min$^{-1}$. The signals at *m/z* of 44 ($C_3H_8$), 42($C_3H_6$), 2 ($H_2$), and 40 (Ar) were collected. The contribution of propane to propene signal was separately determined using a calibration mixture with 10vol% $C_3H_8$ in Ar and subtracted from the overall signal at m/z of 42.

X-ray photoelectron (XP) spectroscopy was applied for catalyst surface characterization using an ESCALAB 220iXL (Thermo Fisher Scientific) set-up with monochromatic Al Kα radiation (E =1486.6 eV). The samples were prepared on a stainless-steel holder with conductive double-sided adhesive carbon tape. The electron binding energies were obtained with charge compensation using a flood electron source and referenced to the C 1s core level of adventitious carbon at 284.8 eV (C−C and C−H bonds).

XRD powder patterns were recorded on a Panalytical X'Pert θ/2θ diffractometer equipped with Xcelerator detector using automatic divergence slits and Cu kα1/α2 radiation (40 kV, 40 mA; λ= 0.15406 nm, 0.154443 nm). Cu beta-radiation was excluded using a nickel filter foil. The measurements were performed with 0.021°$s^{-1}$, respectively. Finely pestled samples were mounted on silicon zero background holders. Reflection intensities obtained after data collection were converted from automatic to fixed divergence slits (0.25°) for further analysis. Reflection positions and profiles were fitted with Pseudo-Voigt function using the HighScore Plus software package (Panalytical). Phase identification was done using the PDF-2 database of the International Center of Diffraction Data (ICDD).

High-resolution electron transmission microscopy (HRTEM) was conducted on an FEI Talos 200X with a working voltage of 200 kV to identify the microstructure and element distribution of fresh catalysts.

X-ray absorption spectra at the Co K absorption edge were recorded at the P65 beamline of PETRA III synchrotron radiation source (DESY, Hamburg) in transmission mode. Higher harmonics were rejected by a pair of Si plane mirrors installed in front of the monochromator. The energy of the X-ray photons was further selected by a Si(111) double-crystal monochromator and the beam size was set by means of slits to 0.4 (vertical) x 2.0 (horizontal) $mm^2$. The spectra were normalized and the extended X-ray absorption fine structure spectra (EXAFS) background was subtracted using the ATHENA program from the IFEFIT software package[28]. The $k^2$-weighted EXAFS functions were Fourier transformed (FT) in the $k$ range of 3.0-10.75$Å^{-1}$ and multiplied by a Hanning window with sill size of 1 $Å^{-1}$. The FT EXAFS spectra were not corrected for the phase shift. The fitting was performed in the r-space on $k^1$, $k^2$-weighted data in the r-range of 1.0-3.3 Å. Co foil as a reference compound was used to establish the value of the reduction factor $S_0^2$. For this purpose, the correlation between $S_0^2$ and the $\sigma^2$ was determined under differently weighted functions $k^n\chi(k)$ (n = 0, 1, 2), which was obtained from modeling the first coordination sphere of Co foil. The crossing region of these curves was centered to obtain the value. This $S_0^2 = 0.78$ was fixed in the following refinement of the $Co/ZrO_2$ atomic structure.

Mechanistic and kinetic aspects of $C_3H_8$ dehydrogenation were studied in the temporal analysis of products (TAP-2) reactor, a pulse technique with a sub-millisecond resolution[29-31]. In these experiments, $1Co/ZrO_2$ (72 mg), $1Co/SiO_2$ (26 mg) or $ZrO_2$ (72 mg) of 315 - 710 μm fraction was loaded in a quartz-tube reactor and fixed within its isothermal zone between two layers of quartz particles of 250-355 μm size. The catalysts were initially treated in a flow containing 50% $H_2$ in $N_2$ with a total flow rate of 8 ml/min at 550 or 600°C to mimic the catalyst state under reaction conditions. Then the reactor was evacuated to ca. $10^{-5}$ Pa and single pulsing of $C_3H_8$:Ar = 1:1 mixture was performed at the pretreatment temperature. The total pulse size was $0.4\text{-}1.6\cdot10^{16}$ molecules. The inlet feed and the effluent gases were quantitatively analyzed by a quadrupole mass spectrometer (HAL RC 301 Hiden Analytical). The following *m/z* values were used for mass-spectrometric identification of different compounds: 44 ($CO_2$, $C_3H_8$), 42 ($C_3H_8$, $C_3H_6$), 41 ($C_3H_8$, $C_3H_6$), 30 ($C_2H_6$), 29 ($C_3H_6$, $C_2H_6$), 28 ($C_3H_6$, $C_2H_6$, $C_2H_4$, CO, $CO_2$), 26 ($C_3H_6$, $C_2H_6$, $C_2H_4$), 18($H_2O$), 2 ($H_2$) and 40 (Ar). Pulses

were repeated 10 times for each *m/z* value and averaged to improve the signal-to-noise ratio. The concentration of the feed and the outlet gases was calculated from the areas of signals recorded at the respective *m/z* values using standard fragmentation patterns and sensitivity factors determined in separate experiments.

The recorded responses were normalized for an easier comparison of the position of the maximal concentration ($t_{max}$) of the feed components and the reaction products. The experimental time was transformed into a dimensionless time using equation 1 as recommended in Ref.[31] to consider the different diffusion velocities of $C_3H_8$, $C_3H_6$ and $H_2$.

$$Dimensionless\ time = \frac{t \times D^{eff}_{Knudsen}(i)}{L^2} \quad (1)$$

Where t is the experimental time, $D^{eff}_{Knudsen}$ (i) is the diffusion coefficient of $C_3H_8$, $C_3H_6$, $H_2$ or Ar and L is the diffusion length. The diffusion length for $C_3H_8$ corresponded to the whole reactor length, while for the reaction products $C_3H_6$ and $H_2$ it was equal to the distance from the beginning of the catalyst layer to the reactor outlet. The diffusion coefficients of $C_3H_8$, $C_3H_6$ and $H_2$ were calculated from that of Ar according to equation 2. The diffusion coefficient of Ar was determined through fitting the experimental response of this gas to the Knudsen diffusion model[32].

$$D^{eff}_{Knudsen}(i) = D^{eff}_{Knudsen}(Ar) \times \sqrt{\frac{M(Ar)}{M(i)}} \quad (2)$$

### *2.3 Catalytic Tests*

All catalytic tests were carried out at 550°C and 1 bar in an in-house developed setup consisting of 15 continuous-flow fixed-bed quartz reactors. The rate of propene formation was determined at a degree of propane conversion below 10% after the first 300 s on propane stream. Typically, the catalysts (25 mg, fraction of 315-710µm) were heated to 550°C in $N_2$ flow with a heating rate of 10 K·min$^{-1}$ and then treated in air for 1 h. Hereafter, they were flushed with $N_2$ for 15 min, reduced with 40vol%$H_2$/Ar (10 mL·min$^{-1}$) for 30min and exposed to a flow (20 mL·min$^{-1}$) of 40vol%$C_3H_8$/$N_2$.

To determine an apparent activation energy of propene formation in the temperature range of 500-545°C, catalytic tests were carried out at propane conversion below 10%. To this end, the catalyst amount and the total feed flow were varied from 25 to 50 mg and from 10 to 30 mL·min$^{-1}$, respectively.

The long-term stability of 1Co/$ZrO_2$ was investigated in a series of 10 PDH/regeneration cycles performed at 550°C using a flow (10 mL·min$^{-1}$) of 40vol%$C_3H_8$/$N_2$. The catalyst amount was set at 125 mg. Prior to the first PDH cycle, the catalyst was heated to 550°C in $N_2$ flow and then calcined in air for 1h followed by feeding $N_2$ for 15 min to remove air. Hereafter, the propane-containing reaction mixture was fed for 50 min. The reaction feed was then replaced by a flow of $N_2$ for 15 min before feeding air for catalyst regeneration for 30 min. The regeneration and PDH cycles were separated by a purging step in $N_2$ flow for 15 min.

An on-line gas chromatograph (Agilent 6890) equipped with PLOT/Q (for $CO_2$), AL/S (for hydrocarbons), and Molsieve 5 (for $H_2$, $O_2$, $N_2$ and CO) columns as well as flame ionization and thermal conductivity detectors was used for quantifying the concentration of the feed components and the reaction products. The feed components and reaction products

were analyzed every 5 min.

Equations 3-5 were used for calculating the initial rate of propene formation ($r(C_3H_6)$), propane conversion ($X(C_3H_8)$) and selectivity to gas-phase products ($S_i$), respectively. The turnover frequency (TOF) of propene formation with respect to Co was calculated according to equation 6.

$$r(C_3H_6) = \frac{\dot{n}^{out}_{C_3H_6}}{m_{cat}} \quad (3)$$

$$X(C_3H_8) = \frac{\dot{n}^{in}_{C_3H_8} - \dot{n}^{out}_{C_3H_8}}{\dot{n}^{in}_{C_3H_8}} \quad (4)$$

$$S_i = \frac{v_{C_3H_8}}{v_i} \times \frac{\dot{n}^{out}_i}{\dot{n}^{in}_{C_3H_8} - \dot{n}^{out}_{C_3H_8}} \quad (5)$$

$$TOF_{Co}(C_3H_6) = \frac{r(C_3H_6)}{N_{Co} \times 60} \quad (6)$$

$\dot{n}$ ($\dot{n}_i$ or $\dot{n}_{C_3H_8}$) with superscripts *in* or *out* stands for the molar flows of gas-phase components at the reactor inlet or outlet. Here, $v_i$ is the stoichiometric coefficient for product *i*. $N_2$ was used as internal standard to consider reaction-induced changes in the number of moles. $N_{Co}$ stands for the number of cobalt moles per gram of catalyst.

## 3 Results and discussion

### *3.1 Catalysts and their characterization*

XRD patterns of bare $ZrO_2$ and Co-containing samples are presented in Figure 1(a). The tetragonal $ZrO_2$ phase was identified after the introduction of cobalt into the monoclinic $ZrO_2$ phase, suggesting that the incorporation of cobalt into the $ZrO_2$ lattice leads to such a phase transformation (Figure S1(a))[24]. No obvious diffraction peaks related to a $CoO_x$-containing phase were observed in the XRD patterns of $Co/ZrO_2$ samples with Co loading below 1 wt%. However, when the Co content was 3wt%, a diffraction peak appeared at 2θ of 36.87°, which is attributed to the $Co_3O_4$ phase (Figure S1(b))[33].

The UV-vis spectra of all samples are characterized by two absorption bands at 227 and 263 nm (Figure 1(b)), which can be attributed to the monoclinic $ZrO_2$ phase[34]. The bands at approximately 509 and 620 nm are present in the spectrum of $1Co/ZrO_2$ and have been assigned to the $v_3$ ($4A_2 \rightarrow {}^4T_1(P)$) transition, which is characteristic of pseudo-tetrahedral $Co^{2+}$ species[16]. Obvious broad absorption bands at 450 and 753 nm were identified in the spectrum of $3Co/ZrO_2$. They are attributed to the ligand-to-metal charge transfer of $O^{2-} \rightarrow Co^{2+}$ and $O^{2-} \rightarrow Co^{3+}$ in the spinel $Co_3O_4$ [16, 19]. The UV-vis results are consistent with the XRD data. Thus, the structure of $CoO_x$ evolves from highly dispersed to agglomerated $CoO_x$/crystalline $Co_3O_4$ with increasing metal loading.

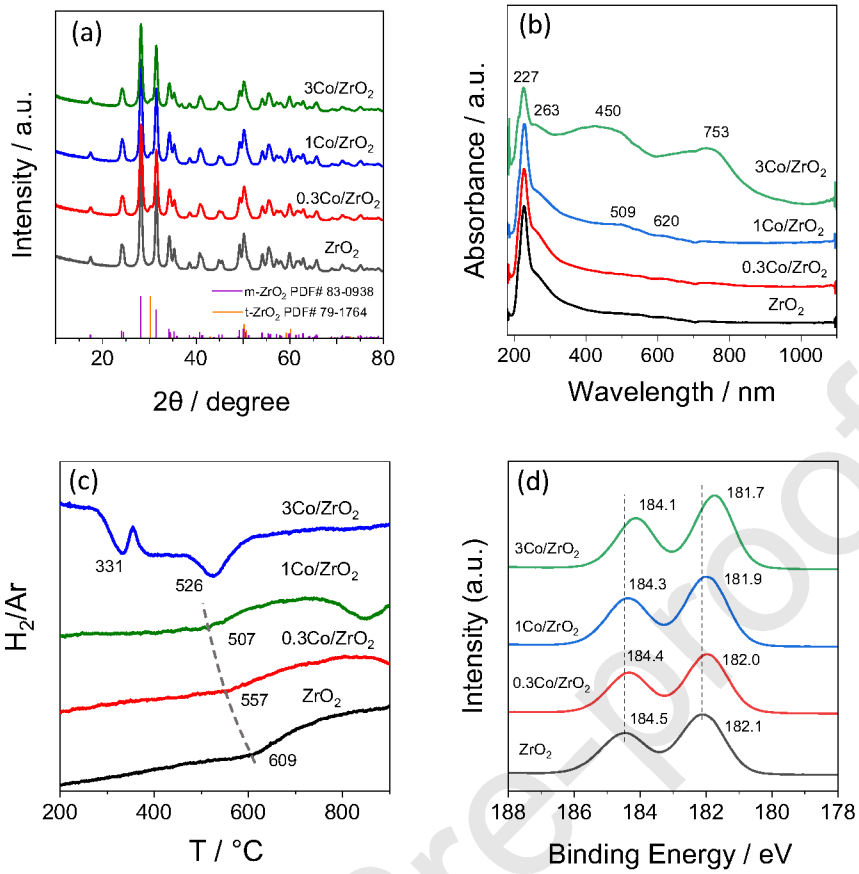


Figure 1. (a) XRD patterns, (b) UV-vis spectra, (c) $H_2$-TPR profiles and (d) XP spectra of Zr 3d of bare $ZrO_2$ and differently loaded $xCo/ZrO_2$ samples.

The acidic properties of the catalysts were characterized by $NH_3$-TPD tests (Figure S2). The number of acidic sites per gram of catalyst (N (a.s.)) was calculated by integrating the $NH_3$ profiles over the whole temperature range. It decreases with an increase in Co content (Table S1). The decrease can be explained by the participation of acidic zirconia sites in the anchoring of $CoO_x$ species.

The cobalt promoter and its content are important for the redox properties of the catalysts as determined by $H_2$-TPR tests (Figure 1(c)). Only one $H_2$ consumption peak at around 609°C was identified in the $H_2$-TPR profile of bare $ZrO_2$. It can be assigned to the reaction of hydrogen with lattice oxygen of zirconia[24, 26, 27]. The profiles of $0.3Co/ZrO_2$ and $1Co/ZrO_2$ are characterized by two resolved $H_2$ consumption peaks between 500-600°C and above 800°C. The intensity of the first peak does not depend on the cobalt loading, while the position is shifted to lower temperatures in comparison with bare $ZrO_2$. Therefore, this peak should be assigned to the reaction of hydrogen with surface lattice oxygen of zirconia. As the intensity of the $H_2$ consumption peak above 800°C increases with cobalt loading, this process can be attributed to the reduction of $CoO_x$ species in the zirconia matrix[35]. For $3Co/ZrO_2$, two obvious $H_2$ consumption peaks were observed at 331 and 526°C. The former peak belongs to the reduction of $Co^{3+}$ to $Co^{2+}$ in $Co_3O_4$, while the latter peak should assigned to the removal of lattice oxygen from $ZrO_2$ and to the reduction of $Co^{2+}$ to $Co^0$[36]. Based on the above discussion, we can conclude that the peaks of $H_2$ consumption at 557 and 507°C in the $H_2$-TPR profiles of $0.3Co/ZrO_2$ and $1Co/ZrO_2$, respectively, should be attributed to the

reaction of hydrogen with lattice oxygen of zirconia. Since this reduction process occurs at lower temperatures in the $Co/ZrO_2$ samples than in bare $ZrO_2$, the cobalt promoter enhances the releasability of lattice oxygen from $ZrO_2$.

X-ray photoelectron spectroscopy is a powerful technique to characterize the chemical electronic states of elements on the surface of catalysts. Thus, it has been applied to check if there is any interplay between Co and $ZrO_2$. The XP spectra of Zr 3d of selected catalysts are shown in Figure 1(d). The binding energies at 182.1 and 184.5 eV in the spectrum of bare $ZrO_2$ can be assigned to the Zr $3d_{5/2}$ and Zr $3d_{3/2}$, respectively, and were related to $Zr^{4+}$ sites. Noticeably, the Zr 3d binding energies of $Co/ZrO_2$ samples are shifted to lower values with increasing Co loading (Figure 1(d)), while the binding energy of Co $2p_{3/2}$ increases (Figure S3). Such changes suggest that the electronic density of $Zr^{4+}$ increases in the presence of cobalt. This can be explained by a formal electron transfer from $Co^{2+}$ to $Zr^{4+}$, resulting in an electron enrichment around the latter.

High-resolution transmission electron microscopy (HRTEM) was used to derive insight into the distribution of Co species in the $1Co/ZrO_2$ catalyst. No obvious $CoO_x$ particles and clusters could be identified on the surface of this catalyst (Figure 2a). EDS mapping was also used and suggests that Co is distributed uniformly (Figure 2 b-e). This conclusion is also consistent with the XRD and UV-vis results.

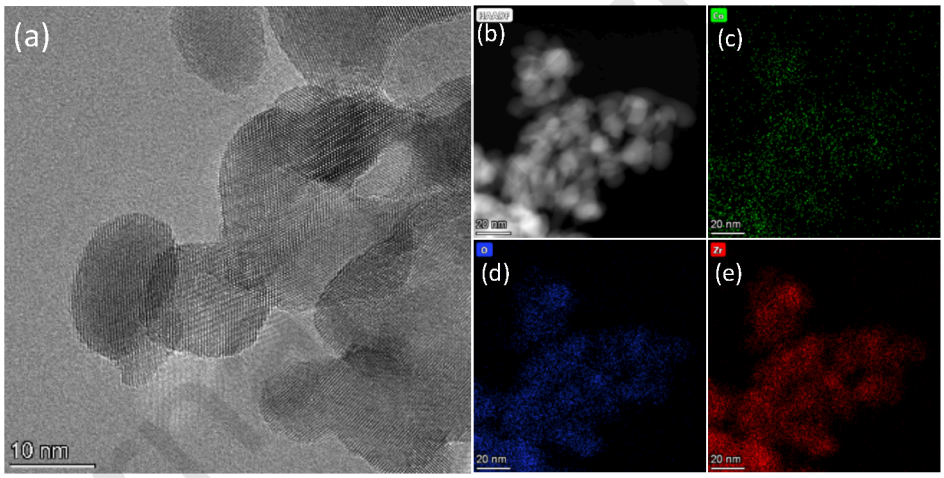


Figure 2. (a) HRTEM image and (b-e) energy-dispersive X-ray (EDX) mapping of $1Co/ZrO_2$.

Figure 3(a) shows the X-ray absorption near-edge structure (XANES) spectra of the $1Co/ZrO_2$ catalyst together with some reference materials. The pre-edge peak at 7709.5 eV indicates that cobalt in the catalyst is present in the form of $Co^{2+}$[15, 16]. The Fourier transform (FT) $k^2$-weighted extended X-ray absorption fine structure (EXAFS) spectrum of $1Co/ZrO_2$ differs from that of Co foil, CoO and $Co_3O_4$ (Figure 3 (b)). Thus, the catalyst possesses a uniquely structured $CoO_x$ species. The signal at ~1.5 Å in the EXAFS spectrum of $1Co/ZrO_2$ is typical for the first shell Co-O scattering. In addition, a small signal at 2.5 Å is also observed in this spectrum. This is probably due to second shell scattering that corresponds to $Zr^{4+}$ neighbors. On this basis, we suppose the formation of isolated $Co^{2+}$ cations on the $ZrO_2$ surface.

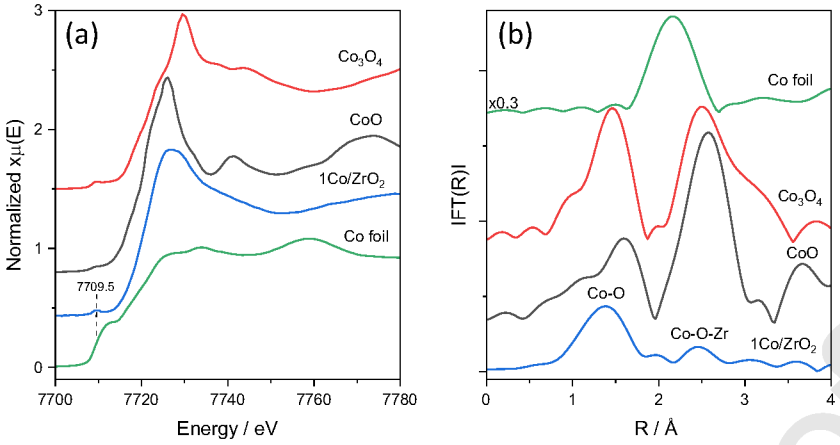


Figure 3. Co K-edge (a) XANES and (b) EXAFS spectra of the $1Co/ZrO_2$ sample, Co foil, CoO and $Co_3O_4$ oxides.

According to the fit of EXAFS spectra (Table S2, Figure S4), a single atom model of $Co^{2+}$ in $1Co/ZrO_2$ is more suitable than a $CoO_x$-cluster model. There are two Co-O bonds with the length of 1.92 and 2.12 Å and two additional Co-O-Zr bonds with the length of 2.65 and 3.2 Å. A previous study [35] concluded that $CoO_x$ single atoms incorporated into the lattice of $ZrO_2$ have Co-O (1.88 Å) and Co-O-Zr bonds (2.71 Å). The short Co-O-Zr bond was explained by the fact that when $Co^{2+}$ replaces one $Zr^{4+}$ cation in the lattice of $ZrO_2$ its position is shifted in comparison with the regular $Zr^{4+}$ position. The Co-O (1.92 Å) and Co-O-Zr (2.65 Å) bond lengths determined in the present study are very similar to those in Ref.[35]. Thus, both the latter and our present data suggest that single $Co^{2+}$ species are incorporated into the lattice of $ZrO_2$. The longer Co-O bond with the length of 2.09 Å might be attributed to additional bonds of Co with surface -OH hydroxy species or adsorbed $H_2O$[37].

### *3.2 Catalyst activity and kind of active sites*

The rate of propene formation over bare $ZrO_2$ and differently loaded $xCo/ZrO_2$ catalysts is shown in Figure 4a. The activity significantly increased after promoting of $ZrO_2$ with cobalt and reached its maximum value of 1.2 $mmol \cdot g^{-1} \cdot min^{-1}$ at a Co loading of 1 wt%. Noticeably, this activity was even superior to that of a commercial analogue of $K\text{-}CrO_x/Al_2O_3$. When the Co loading was increased to 3 wt%, the activity sightly decreased probably due to the formation of large crystallites of $Co_3O_4$ as evidenced by XRD and UV-vis spectroscopy (Figure 1a). Crystalline $Co_3O_4$ is active for cracking and coke formation but inactive for the PDH reaction[23].

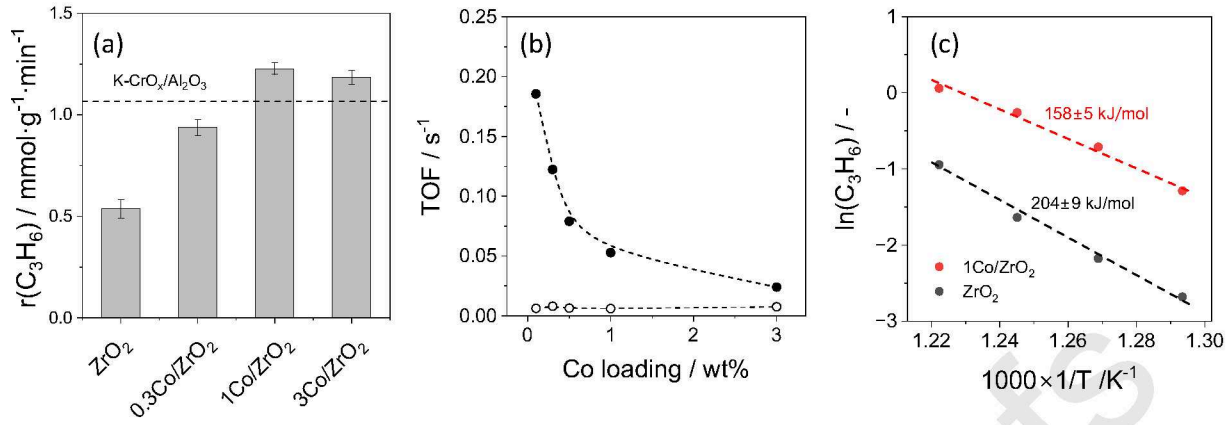


Figure 4. (a) The rate of propene formation over bare $ZrO_2$ and $xCo/ZrO_2$ with different cobalt contents. The grey dashed line in (a) stands for the activity of a commercial-like $K\text{-}CrO_x/Al_2O_3$. (b) The effect of Co loading on Co-related TOF value. $Co/ZrO_2$(●), $Co/SiO_2$(○). Reaction conditions: T=550°C, catalyst amount=25mg, WHSV($C_3H_8$)=37.7 $h^{-1}$, $C_3H_8$:$N_2$=2:3. (c) Arrhenius plots for propene formation over $1Co/ZrO_2$ and bare $ZrO_2$ as well as the therefrom calculated apparent activation energy.

To check if $Co^{2+}$ sites are the only active species in the $Co/ZrO_2$ catalysts, an apparent Co-related turn-over frequency (TOF) of propene formation was calculated (Figure 4b). The TOF value decreases from 0.19 to 0.02 $s^{-1}$ with an increase in Co loading from 0.1 to 3 wt%. Therefore, we can exclude $Co^{2+}$ as the only active species. Importantly, the TOF values of $Co/SiO_2$ catalysts do not depend on Co loading, indicating that $CoO_x$ is the only active species of these catalysts. The effect of the kind of support on the dependence of Co-related TOF on cobalt loading suggests that $ZrO_2$ must be involved in the PDH reaction over the $Co/ZrO_2$ catalysts due to the presence of coordinatively unsaturated zirconium cations ($Zr_{cus}$). Such sites are formed *in situ* under PDH conditions via removal of surface lattice oxygen of $ZrO_2$. Our $H_2$-TPR tests have shown that this process is facilitated in the presence of cobalt in $ZrO_2$ (Figure 1c).

Although $Zr_{cus}$ sites are directly involved in the PDH reaction over $ZrO_2$ and $Co/ZrO_2$, they differ in their intrinsic activity as we could conclude from our kinetic measurements at different reaction temperatures. The therefrom determined apparent activation energy ($E_a$) values of propene formation over $1Co/ZrO_2$ and bare $ZrO_2$ are 158 ±5 kJ·$mol^{-1}$ versus 204±9 kJ·$mol^{-1}$, respectively (Figure 4c). Thus, the presence of $Co^{2+}$ in the lattice of $ZrO_2$ should affect the activity of $Zr_{cus}$ to dehydrogenate propane. This statement is indirectly supported by the following result. The rate of propene formation over $1Co/ZrO_2$ is higher than the sum of the rates determined separately over bare $ZrO_2$ ($Zr_{cus}$ is the only active site) and $1Co/SiO_2$ ($CoO_x$ is the only active species) as shown in Figure S5. As $CoO_x$ was excluded (see previous paragraph) as the active species of the $Co/ZrO_2$ catalysts, the promotor should affect the intrinsic activity of $Zr_{cus}$. If it did not impact this catalyst property, there would be no difference in the Ea values of propene formation over $ZrO_2$ and $1Co/ZrO_2$. The promoter can also influence the concentration of such sites. Therefore, the synergistic effect between $CoO_x$ and $ZrO_2$ can be explained by improving the reducibility of $ZrO_2$ (Figure 1c) and the intrinsic activity of $Zr_{cus}$ sites (Figure 4c).

### 3.3 *Rate-determining step*

To gain a deeper insight into the positive role of cobalt promoter on PDH activity of $Zr_{cus}$, propane temperature-programmed surface reaction ($C_3H_8$-TPSR) experiments were carried out using $1Co/ZrO_2$ and bare $ZrO_2$. The temperature, at which the intensity of the $C_3H_8$ signal begins to decrease, is defined as the C–H activation temperature. It is around 449°C for $1Co/ZrO_2$ (Figure S6(a)). The corresponding value for $ZrO_2$ is 490°C. Thus, propane activation occurs more readily on $1Co/ZrO_2$. It is also important to highlight that the temperature, at which propene appears in the gas phase, was lower than the temperature, at which gas-phase $H_2$ was detected (Figure S6(b-e)). This implies that $H_2$ formation should be the rate-limiting step in the PDH process.

Further insights into the rates of formation of $C_3H_6$ and $H_2$ were derived from pulse experiments with a $C_3H_8$:Ar = 1:1mixture in the temporal analysis of products reactor at 550 and 600°C. In these experiments, $C_3H_6$ and $H_2$ were formed over $1Co/ZrO_2$ and $ZrO_2$ at both temperatures, whereas $1Co/SiO_2$ formed these products only at 600°C. The transient responses recorded at 600°C are shown in Figure S7. The responses of $C_3H_6$ and $H_2$ are broader than that of $C_3H_8$ indicating that these substances are products of $C_3H_8$ dehydrogenation. Moreover, the transient response of hydrogen is significantly broader than that of propene for all catalysts, indicating that in agreement with the results of $C_3H_8$-TPSR, the dehydrogenation of propane is limited by $H_2$ formation. Despite a similar arrangement, the responses differ in their broadness and the position of the maximal concentration, i.e., the rates of $C_3H_6$ and $H_2$ formation depend on the catalyst. To quantify this difference, we plot the difference between the $t_{max}(H_2$ or $C_3H_6)$ and $t_{max}(Ar)$ values ($t_{max}(H_2$ or $C_3H_6)$ - $t_{max}(Ar)$) vs. the catalyst (Figure 5). Subtracting $t_{max}(Ar)$ should reduce the contribution of the different densities of the reactor charges to the position of the response maxima since a higher density slows down the diffusion through the reactor.

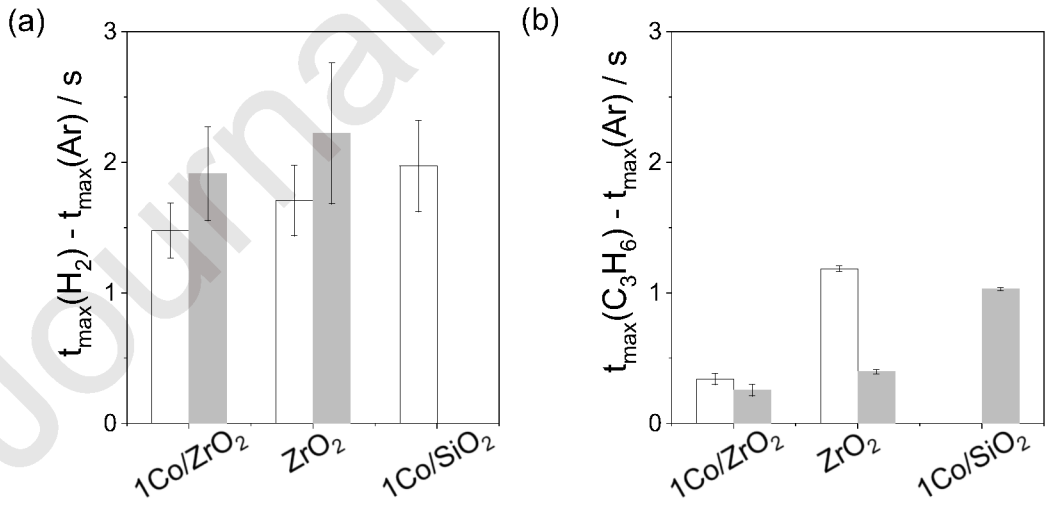


Figure 5. (a) $t_{max}(H_2)$ - $t_{max}(Ar)$ and (b) $t_{max}(C_3H_6)$ - $t_{max}(Ar)$ values obtained upon pulsing $C_3H_8$:Ar = 1:1 mixture at 550 (white bars) and 600°C (grey bars) vs. catalyst.

As expected from the temperature dependance of the reaction rate, the $t_{max}$ values of both products of propane dehydrogenation drop upon temperature increase to 600°C. The $t_{max}$ values for $C_3H_6$ are lower than those for $H_2$, highlighting the faster formation of the olefine in

comparison with the formation of $H_2$. Thus, the latter process and not the cleavage of CH bonds in propane limits the rate of propene formation. Independently from the reaction temperature, $1Co/ZrO_2$ possesses lower $t_{max}$ values of $C_3H_6$ and $H_2$ than those of bare $ZrO_2$, whereas $1Co/SiO_2$ is characterized by the highest $t_{max}$ values. Therefore, considering the low rate of $C_3H_8$ dehydrogenation over $CoO_x$ in $1Co/SiO_2$, its deposition over $ZrO_2$ results in a synergistic between these components, which is responsible for accelerating the rates of $C_3H_6$ and $H_2$ formation.

### *3.4 Durability tests*

The practical relevance of the most promising $1Co/ZrO_2$ catalyst was demonstrated in a series of 10 PDH reaction-regeneration cycles under industrially relevant conditions (Figure 6). The reaction was performed at 550°C and lasted for 50 min using a feed with 40vol% $C_3H_8$. The regeneration stage implied calcination of spent catalyst in air at 550 for 30 min. The initial $C_3H_8$ conversion was about 24% and the corresponding selectivity to propene was higher than 80%. The conversion gradually decreased to 7%, while the selectivity did not strongly change with time on stream. In contrast to previously developed supported $CrO_x/LaZrO_x$[38], the present catalyst could restore its initial conversion completely after the oxidative catalyst regeneration. There were no obvious changes in the profiles of propane conversion and propene selectivity during 10 PDH/oxidative regeneration cycles. Thus, no activity-affecting structural changes occurred under reaction or regeneration conditions.

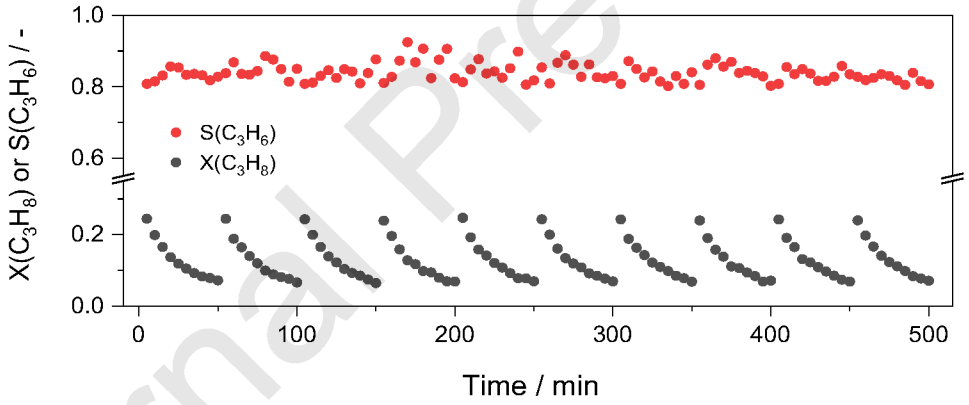


Figure 6. Propane conversion and the selectivity to propene over $1Co/ZrO_2$ in 10 PDH/ regeneration cycles. Reaction conditions: T=550°C, catalyst amount=125mg, WHSV($C_3H_8$)=3.8 $h^{-1}$, $C_3H_8$:$N_2$=2:3. Each cycle consisted of a PDH stage lasted for 50 min and a regeneration stage lasted for 30 min.

The catalyst stability against reaction-induced restructuring was independently confirmed by means of HRTEM analysis and EDS mapping of a spent $1Co/ZrO_2$ sample (after 10 cycles) (Figure S8). The catalyst deactivation within each PDH cycle is mainly caused by the deposition of coke which can be easily oxidized.

We also benchmarked the developed catalyst against Co-based catalysts in terms of space-time yield of propene formation (STY($C_3H_6$)). The initial STY($C_3H_6$) value of 0.71 $kg \cdot h^{-1} \cdot kg_{cat}^{-1}$ was achieved at 57% equilibrium propane conversion at 550°C. This value is higher than those reported for most previously developed catalysts tested at the same or higher temperatures (Figure S9).

## 4 Conclusions

Promoting $ZrO_2$ with $CoO_x$ by a simple impregnation method yields active catalysts for non-oxidative dehydrogenation of propane to propene. When the promoter forms a solid solution with $ZrO_2$ on the surface, it is stabilized as $Co^{2+}$ in the lattice of the host oxide resulting in the formation of coordinatively unsaturated $Zr^{4+}$ sites ($Zr_{cus}$). The activity of the latter in the PDH reaction increases strongly in the presence of $Co^{2+}$ and is significantly higher than the sum of activities of $Co^{2+}$ sites on $SiO_2$ and $Zr_{cus}$ in unpromoted $ZrO_2$. The presence of $Co_3O_4$ must be avoided to achieve high activity. The synergistic effect between $Co^{2+}$ and $Zr_{cus}$ is related to enhancing the rates of CH bonds cleavage in propane and recombination of surface hydrogen species formed from propane. The latter process is the rate-limiting step in the course of the PDH reaction. The derived knowledge related to the synergistic effect provides the basis for rational design of PDH metal-oxide-based catalysts with industrially relevant performance.

## Acknowledgements

Financial support by the State of Mecklenburg-Vorpommern is gratefully acknowledged. This work is supported by the National Natural Science Foundation of China (Grant Nos. 22225807, 21961132026). We acknowledge DESY (Hamburg, Germany), a member of the Helmholtz Association HGF, for the prevision of experimental facilities. Parts of this research were carried out at PETRA III, and we would like to thank Dr. Edmund Welter for assistance in using beamlineP65.

## References

[1] T. Otroshchenko, G.Y. Jiang, V.A. Kondratenko, U. Rodemerck, E.V. Kondratenko, Current status and perspectives in oxidative, non-oxidative and $CO_2$-mediated dehydrogenation of propane and isobutane over metal oxide catalysts, Chem. Soc. Rev, 50 (2021) 473-527.

[2] S. Chen, X. Chang, G. Sun, T. Zhang, Y. Xu, Y. Wang, C. Pei, J. Gong, Propane dehydrogenation: catalyst development, new chemistry, and emerging technologies, Chem. Soc. Rev, 50 (2021) 3315-3354.

[3] Y. Dai, X. Gao, Q. Wang, X. Wan, C. Zhou, Y. Yang, Recent progress in heterogeneous metal and metal oxide catalysts for direct dehydrogenation of ethane and propane, Chem Soc Rev, 50 (2021) 5590-5630.

[4] J.J.H.B. Sattler, J. Ruiz-Martinez, E. Santillan-Jimenez, B.M. Weckhuysen, Catalytic dehydrogenation of light alkanes on metals and metal oxides, Chem. Rev., 114 (2014) 10613-10653.

[5] S.M. Sadrameli, Thermal/catalytic cracking of liquid hydrocarbons for the production of olefins: A state-of-the-art review II: Catalytic cracking review, Fuel, 173 (2016) 285-297.

[6] S. Lwin, I.E. Wachs, Olefin Metathesis by Supported Metal Oxide Catalysts, ACS Catal., 4 (2014) 2505-2520.

[7] J.C. Mol, Industrial applications of olefin metathesis, J. Mol. Catal. A: Chem., 213 (2004) 39-45

[8] Q. Zhang, T. Xiao, C. Liu, T. Otroshchenko, E.V. Kondratenko, Performance Descriptors for Catalysts Based on Molybdenum, Tungsten, or Rhenium Oxides for Metathesis of Ethylene with 2-Butenes to Propene, Angew. Chem. Int. Ed., (2023) e202308872.

[9] Q. Zhang, T. Otroshchenko, E.V. Kondratenko, Fundamentals and application potential of the synergy effect between ZnO and $Mo/SiO_2$ for propene production in the metathesis of ethylene and trans-2-butene, Catal. Sci. Tech., 12 (2022) 5210-5216.

[10] Q. Zhang, J. Rabeah, T.H. Vuong, T. Otroshchenko, E.V. Kondratenko, Effect of $AlSiO_x$ support modification by alkali or alkaline earth metals on propene formation in the metathesis of $C_2H_4$ and 2-C $_4H_8$ over $MoO_x$-based catalysts, Catal. Sci. Tech., (2023) 767-773.

[11] D. Zhao, X. Tian, D.E. Doronkin, S. Han, V.A. Kondratenko, J.-D. Grunwaldt, A. Perechodjuk, T.H. Vuong, J. Rabeah, R. Eckelt, H. Jiao, G. Jiang, E.V. Kondratenko, In situ formation of ZnOx species for efficient propane dehydrogenation, Nature, 599 (2021) 234-238.

[12] Z. Huang, D. He, W. Deng, G. Jin, K. Li, Y. Luo, Illustrating new understanding of adsorbed water on silica for inducing tetrahedral cobalt (II) for propane dehydrogenation, Nat. Commun, 14 (2023) 100

[13] W. Wang, Y. Wu, T. Liu, Y. Zhao, Y. Qu, R. Yang, Z. Xue, Z. Wang, F. Zhou, J. Long, Z. Yang, X. Han, Y. Lin, M. Chen, L. Zheng, H. Zhou, X. Lin, F. Wu, H. Wang, Y. Yang, Y. Li, Y. Dai, Y. Wu, Single Co Sites in Ordered SiO2 Channels for Boosting Nonoxidative Propane Dehydrogenation, ACS Catal., (2022) 2632-2638.

[14] S. Song, J. Li, Z. Wu, P. Zhang, Y. Sun, W. Song, Z. Li, J. Liu, In situ encapsulated subnanometric CoO clusters within silicalite-1 zeolite for efficient propane dehydrogenation, AlChE J., 68 (2022) 1-11.

[15] Z.P. Hu, G. Qin, J. Han, W. Zhang, N. Wang, Y. Zheng, Q. Jiang, T. Ji, Z.Y. Yuan, J. Xiao, Y. Wei, Z. Liu, Atomic Insight into the Local Structure and Microenvironment of Isolated Co-Motifs in MFI Zeolite Frameworks for Propane Dehydrogenation, J.Am.Chem.Soc., 144 (2022) 12127-12137.

[16] L. Wu, Z. Ren, Y. He, M. Yang, Y. Yu, Y. Liu, L. Tan, Y. Tang, Atomically Dispersed $Co^{2+}$ Sites Incorporated into a Silicalite-1 Zeolite Framework as a High-Performance and Coking-Resistant Catalyst for Propane Nonoxidative Dehydrogenation to Propylene, ACS Appl Mater Interfaces, 13 (2021) 48934-48948.

[17] Y. Dai, Y. Wu, H. Dai, X. Gao, S. Tian, J. Gu, X. Yi, A. Zheng, Y. Yang, Effect of coking and propylene adsorption on enhanced stability for Co2+-catalyzed propane dehydrogenation, J. Catal., 395 (2021) 105-116.

[18] Z. Bian, N. Dewangan, Z. Wang, S. Pati, S. Xi, A. Borgna, H. Kus, S. Kawi, Mesoporous-Silica-Stabilized Cobalt(II) Oxide Nanoclusters for Propane Dehydrogenation, ACS Applied Nano Materials, 4 (2021) 1112-1125.

[19] Y. Dai, J. Gu, S. Tian, Y. Wu, J. Chen, F. Li, Y. Du, L. Peng, W. Ding, Y. Yang, $\gamma$-$Al_2O_3$ sheet-stabilized isolate $Co^{2+}$ for catalytic propane dehydrogenation, J. Catal., 381 (2020) 482-492.

[20] C. Chen, S. Zhang, Z. Wang, Z.-Y. Yuan, Ultrasmall Co confined in the silanols of dealuminated beta zeolite: A highly active and selective catalyst for direct dehydrogenation of propane to propylene, J. Catal., 383 (2020) 77-87.

[21] X. Li, P. Wang, H. Wang, C. Li, Effects of the state of Co species in $Co/Al_2O_3$ catalysts on the catalytic performance of propane dehydrogenation, Appl. Surf. Sci., 441 (2018) 688-693.

[22] B. Hu, A. "Bean" Getsoian, N.M. Schweitzer, U. Das, H. Kim, J. Niklas, O. Poluektov, L.A. Curtiss, P.C. Stair, J.T. Miller, A.S. Hock, Selective propane dehydrogenation with single-site $Co^{II}$ on $SiO_2$ by a non-redox mechanism, J. Catal., 322 (2015) 24-37.

[23] Y. Li, Q. Zhang, S. Fu, V.A. Kondratenko, T. Otroshchenko, S. Bartling, Y. Zhang, A. Zanina, Y. Wang, G. Cui, M. Zhou, Z. Zhao, C. Xu, G. Jiang, E.V. Kondratenko, Active Species and Fundamentals of their Creation in Co-containing Catalysts for Efficient Propane Dehydrogenation to Propylene, Chem. Eng. J., (2023) 141778.

[24] Y. Zhang, Y. Zhao, T. Otroshchenko, H. Lund, M.-M. Pohl, U. Rodemerck, D. Linke, H. Jiao, G. Jiang, E.V. Kondratenko, Control of coordinatively unsaturated Zr sites in $ZrO_2$ for efficient C–H bond activation, Nat. Commun, 9 (2018) 3794.

[25] T. Otroshchenko, S. Sokolov, M. Stoyanova, V.A. Kondratenko, U. Rodemerck, D. Linke, E.V. Kondratenko, $ZrO_2$-based alternatives to conventional propane dehydrogenation catalysts: active sites, design, and performance, Angew. Chem. Int. Ed., 54 (2015) 15880-15883

[26] S. Han, Y. Zhao, T. Otroshchenko, Y. Zhang, D. Zhao, H. Lund, T.H. Vuong, J. Rabeah, U. Bentrup, V.A. Kondratenko, Unraveling the Origins of the Synergy Effect between $ZrO_2$ and $CrO_x$ in Supported $CrZrO_x$ for Propene Formation in Nonoxidative Propane Dehydrogenation, ACS Catal., 10 (2019) 1575-1590

[27] T.P. Otroshchenko, U. Rodemerck, D. Linke, E.V. Kondratenko, Synergy effect between Zr and Cr active sites in binary $CrZrO_x$ or supported $CrO_x/LaZrO_x$: Consequences for catalyst activity, selectivity and durability in non-oxidative propane dehydrogenation, J. Catal., 356 (2017) 197-205

[28] B. Ravel, M. Newville, ATHENA, ARTEMIS, HEPHAESTUS: data analysis for X-ray absorption spectroscopy using IFEFFIT, Journal of synchrotron radiation, 12 (2005) 537-541.

[29] K. Morgan, N. Maguire, R. Fushimi, J. Gleaves, A. Goguet, M. Harold, E.V. Kondratenko, U. Menon, Y. Schuurman, G. Yablonsky, Forty years of temporal analysis of products, Catal. Sci. Tech., 7 (2017) 2416-2439.

[30] J. Pérez-Ramírez, E.V. Kondratenko, Evolution, achievements, and perspectives of the TAP technique, Catal. Today, 121 (2007) 160-169.

[31] J.T. Gleaves, G.S. Yablonskii, P. Phanawadee, Y. Schuurman, TAP-2: An interrogative kinetics approach, Appl.Catal.A, 160 (1997) 55-88.

[32] M. Soick, D. Wolf, M. Baerns, Determination of kinetic parameters for complex heterogeneous catalytic reactions by numerical evaluation of TAP experiments, Chemical engineering science, 55 (2000) 2875-2882.

[33] N. Jeon, J. Oh, A. Tayal, B. Jeong, O. Seo, S. Kim, I. Chung, Y. Yun, Effects of heat-treatment atmosphere and temperature on cobalt species in $Co/Al_2O_3$ catalyst for propane dehydrogenation, J. Catal., 404 (2021) 1007-1016

[34] T.A. Maia, J.M. Assaf, E.M. Assaf, Steam reforming of ethanol for hydrogen production on $Co/CeO_2–ZrO_2$ catalysts prepared by polymerization method, Mater. Chem. Phys., 132 (2012) 1029-1034.

[35] N.H.M. Dostagir, R. Rattanawan, M. Gao, J. Ota, J.-y. Hasegawa, K. Asakura, A. Fukouka, A. Shrotri, Co single atoms in $ZrO_2$ with inherent oxygen vacancies for selective hydrogenation of $CO_2$ to CO, ACS Catal., 11 (2021) 9450-9461.

[36] W. Li, Y. Liu, M. Mu, F. Ding, Z. Liu, X. Guo, C. Song, Organic acid-assisted preparation of highly dispersed $Co/ZrO_2$ catalysts with superior activity for $CO_2$ methanation, Appl. Catal. B, 254 (2019) 531-540

[37] C. Papelis, K.F. Hayes, Distinguishing between interlayer and external sorption sites of clay minerals using X-ray absorption spectroscopy, Colloids and Surfaces A: Physicochemical and Engineering Aspects, 107 (1996) 89-96.

[38] T.P. Otroshchenko, U. Rodemerck, D. Linke, E.V. Kondratenko, Synergy effect between Zr and Cr active sites in binary CrZrOx or supported CrOx/LaZrOx: Consequences for catalyst activity, selectivity and durability in non-oxidative propane dehydrogenation, J. Catal., 356 (2017) 197-205.

# The enhancing effect of $Co^{2+}$ on propane non-oxidative dehydrogenation over supported $Co/ZrO_2$ catalysts

Qiyang Zhang[a†], Yuming Li[a,b†], Tatiana Otroshchenko[a], Vita A. Kondratenko[a], Kai Wu[a], Elizaveta A. Fedorova[a], Dmitry E. Doronkin[c], Stephan Bartling[a], Henrik Lund[a], Guiyuan Jiang[b,*], Evgenii V. Kondratenko[a,*]

[a]*Leibniz-Institut für Katalyse e.V., Albert-Einstein-Str. 29a, D-18059 Rostock, Germany*

[b]*State Key Laboratory of Heavy Oil Processing, China University of Petroleum, Beijing, 102249*

[c]*Institute for Chemical Technology and Polymer Chemistry, and Institute of Catalysis Research and Technology, Karlsruhe Institute of Technology, Kaiserstr. 12, D-76131, Karlsruhe, Germany*

*To whom correspondence should be addressed. E-mail addresses: jianggy@cup.edu.cn (GJ, Evgenii.kondratenko@catalysis.de (EVK)

† These authors contributed equally